Mean-Field Model for Heat Transfer in Multichannel Microreactors

Steffen Hardt
Institut für Nano- und Mikroprozesstechnik, Universität Hannover, 30167 Hannover, Germany

Tobias Baier
Abteilung Fluidik und Simulation, Institut für Mikrotechnik Mainz, 55129 Mainz, Germany

DOI 10.1002/aic.11138
Published online February 27, 2007 in Wiley InterScience (www.interscience.wiley.com).

A reduced-order model is developed, allowing for a fast computation of the temperature field in multichannel microreactors. The model regards the fluid and the solid phase as interpenetrating continua and incorporates heat exchange between the two phases via a heat-transfer coefficient, characteristic for the channel geometry under study. The geometry of the channel walls determines the components of the thermal conductivity tensor, which govern conductive heat transfer to the envelope of the reactor. The mean-field model is solved numerically for a test case inspired from practical applications. Parallel to that, a detailed model based on standard methods of computational fluid dynamics is set up with the purpose to benchmark the results of the mean-field model. This full model incorporates the geometric details of the multichannel reactor and contains considerably more degrees of freedom than the mean-field model, resulting in a computational effort that is larger by at least a factor of several hundred. It is found that the temperature fields computed with the two models agree up to maximum deviations of about 3 K on a scale of 35 K. Thus, the mean-field model appears as an efficient tool to evaluate the thermal performance of multichannel microreactors, especially in the context of parameter studies or system optimization. © 2007 American Institute of Chemical Engineers *AIChE J,* 53: 1006–1016, 2007
Keywords: heat transfer, microreactor, multichannel stack, simulation, model reduction

Introduction

Over the past few years, chemical micro process technology has attracted an increasing attention in science, engineering, and industry. This technology is based on guiding fluids through microchannels, where chemical reactions occur and feed components are converted to specific products. The benefits of conducting chemical reactions in microfluidic devices are manifold, among others an increased product yield, suppression of by-products, or production on demand.[1,2] The physical reason for such an increased performance is often the speed up of heat and mass transfer processes, effects that are discussed at length in the books by Karniadakis et al.[3] or Zohar,[4] along with many other characteristic features of microflows. A generic geometry especially for gas-phase microreactors is that of a multichannel stack, where a number of microstructured platelets are stacked onto each other to form a device with a (large) number of parallel microchannels.[5–8] Such designs have been utilized for various reactions such as oxidations or hydrogenations (for an overview see Hessel et al.[1]).

An important point to consider when designing multichannel stacks is their thermal management. Ideally, the reaction conditions are as uniform as possible, in particular the

Correspondence concerning this article should be addressed to S. Hardt at hardt@nmp.uni-hannover.de.

temperature level should be approximately the same in all the channels. The rate constant of chemical reactions usually has an exponential dependence on temperature, which means that the conversion and selectivity achievable in a microchannel depend strongly on temperature. In a multichannel stack which is not designed as a heat-exchanger reactor, a large portion of the heat created or consumed in the reaction is transported by conduction through the wall material. Thus, the reactor should be designed in such a way so as to ensure fast enough heat conduction to guarantee reaction conditions that are as uniform as possible over the multichannel domain. In that context, numerical computations are a helpful tool to assess the suitability of different alternative designs a priori.

Typically, a numerical evaluation of the flow, thermal, and reaction dynamics is done for a single channel. However, there is thermal coupling between the different channels of a reactor and the thermal boundary conditions to be applied for a single channel are not known in advance. Therefore, single-channel simulations are of limited use, and the temperature distribution in the complete multichannel stack has to be considered when evaluating the performance of a microreactor. It has been noted by a number of authors[9,10] that, owing to the comparatively large share of wall material in microreactors, heat transfer between adjacent microchannels proceeds in a different manner as in macroscopic devices. While macroscopically heat conduction along the solid walls can often be neglected and only heat transfer across the walls has to be considered, longitudinal conduction can play an important role in microdevices. Consequently, heat conduction in all three spatial dimensions has to be incorporated into a model. State-of-the-art tools for Computational Fluid Dynamics (CFD) allow performing 3D simulations of reactive flows in parallel microchannels. In this context, the reactor geometry, including all of the fluid–solid interfaces, is modeled explicitly, resulting in very large computational grids when a multitude of channels has to be considered. When parameter studies or optimization runs need to be performed, the computational burden related to such a full model is usually much too large. Therefore, effective models with a reduced number of degrees of freedom are needed to allow for a fast evaluation of design variants. In that context, the term "degree of freedom" refers to the unknowns of the corresponding mathematical problem, which can be either field values at specific points in space or expansion coefficients for the fields to be computed.

A common way of formulating low-dimensional models (that is, such with a comparatively small numbers of degrees of freedom) for systems of parallel microchannels is to subdivide the multichannel stack into different layers and to define a network of thermal resistors layer by layer. Corresponding models have been developed for stacked microchannel heat sinks being used for the cooling of microelectronic components and take into account the 3-D architecture of the cooling device.[11,12] Alternatively, an averaging approach may be employed where spatially averaged fluid and solid temperature fields are defined, which are coupled via a heat transfer coefficient. Such a model has been developed to compute the temperature distribution in a microchannel heat sink with a single layer of channels,[13,14] that is, effectively a 2-D description with continuous temperature fields for the fluid and the solid phase is used.

As an alternative to these, more empirically-based techniques, low-dimensional models may also be derived in a more formal manner. Model reduction aiming at extracting a computational model with relatively few degrees of freedom from a high-dimensional description has been an active research area in the past decade. A large portion of the work is related to the theory of linear dynamical systems and, on the application side, a focus has been on electrical engineering where, for example, it has been attempted to describe the dynamical behavior of electromagnetic devices using low-dimensional models.[15,16] In this context, the objective is often to model the transfer function relating the output of a system to the source terms acting in this system. In frequency space, the transfer function has a number of zeros and poles, and one goal of model reduction is to preserve as much of this structure as possible in a certain frequency range. For this purpose, techniques such as Padé approximations and the construction of Krylov subspaces are employed (for an overview, see Bai[17]).

In contrast to linear dynamical systems, nonlinear models are often required for systems involving fluid flow. Such nonlinear systems are much more difficult to analyze than their linear counterparts. Nevertheless, also for these types of problems model reduction techniques have been developed, which owing to the complexity of nonlinear differential equations are usually not able to approximate the mathematical structure of the operators involved in an equally reliable manner as in the linear domain. An example for nonlinear model reduction is proper orthogonal decomposition (POD).[18] In POD, it is attempted to determine a low-dimensional subspace, which has the property that the projection of the full solution onto this subspace comes as close as possible to the full solution itself. This method is quite general and can in principle be applied to a large class of nonlinear problems.

A common feature of these techniques for model reduction is their algorithmic approach, i.e. a well-defined mathematical procedure is employed to reduce the number of degrees of freedom of an equation or an operator. In contrast to that, the approach we propose in this paper is rather empirical. Rather than writing down the full-scale model and trying to reduce its degrees of freedom by formal operations, our model is constructed in a manner where we replace the original physical picture by an approximately equivalent picture. The model we present is, to our best knowledge, the first reduced-order model for heat transfer in multichannel microreactors applicable to 3-D geometries. It allows for different temperatures of the fluid and the solid phase, and therefore does not rest on the assumption of thermal equilibrium between the two phases utilized in models of heat transfer in porous media.[19] Based on the mathematical formulation presented in this article, we hope to enable a fast numerical evaluation of heat transfer in 3-D multichannel reactor geometries, especially in view of parameter studies and design optimization.

The Model Equations

A generic geometry of a multichannel microreactor is sketched in Figure 1. Many microchannels, usually several

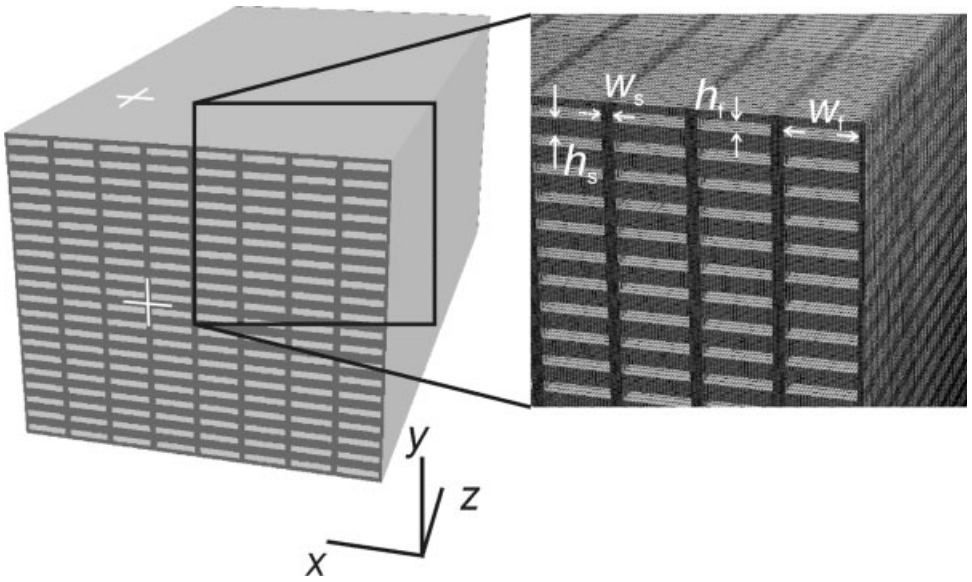

Figure 1. Multichannel stack comprising a large number of microchannels of rectangular cross section.

The white crosses indicate the (x, y) and (x, z) positions corresponding to the plots shown in Figure 5.

hundreds up to several thousands, are arranged in layers stacked onto each other. As a whole, the multichannel stack forms a cuboid of extension L_x, L_y, L_z in x-, y-, and z-direction, respectively. The microchannels of width w_f and depth h_f are assumed to be parallel to the z-axis and are separated by solid walls of thickness w_s and h_s, respectively. The channel walls might be coated with some catalyst medium, or, alternatively, a homogeneous chemical reaction not requiring any catalyst might occur. Usually the multichannel section is embedded in some solid reactor housing containing heating or cooling elements, so it is assumed that the temperature on the envelope of the stack is known. In many cases isothermal boundary conditions should be a reasonable assumption.

The reactor is operated by distributing the reaction fluid over the channels, where either an exo- or an endothermic reaction occurs. The product fluid leaves the reactor and takes away some of the thermal energy. A considerable amount of heat, however, is transported by conduction through the channel walls to the envelope of the multichannel stack. The model presented in the following should be able to reproduce the temperature field in the reactor in an average manner.

The need for modeling single channels and their specific geometry is eliminated when regarding the reaction fluid and wall material as interpenetrating continua. Hence, in the following it is assumed that the reactor stack is filled with interpenetrating fluid and solid phases that interact via the exchange of heat. The volume fractions of these phases can be derived from the geometric parameters h_f, h_s, w_f, and w_s, shown in Figure 1 and are given as

$$\Phi_f = \frac{w_f h_f}{(w_f + w_s)(h_f + h_s)}, \qquad \Phi_s = 1 - \Phi_f. \tag{1}$$

The temperature field of the solid phase can change because of heat conduction or because of heat transfer from the fluid phase. For the fluid, heat conduction is neglected but convective heat transfer due to the flow velocity as well as heat transfer from the solid is taken into account. In the x–y plane no conduction within the fluid without intermediate transfer to the solid walls can occur. The reason for not including fluid heat conduction in z-direction is the fact that in most cases of practical relevance it is negligible when compared with convective transport, an aspect which will be illuminated in some more detail below. The fluid and solid temperature fields T_f and T_s are then obtained as solutions of the equations

$$\rho_f c_f \left(\frac{\partial}{\partial t} + u_i \frac{\partial}{\partial x_i}\right) T_f = -\alpha\, a_v (T_f - T_s) + S_{cf}$$

$$\rho_s c_s \frac{\partial}{\partial t} T_s = \frac{\partial}{\partial x_i}\frac{\partial}{\partial x_j} k_{ij} T_s - \alpha\, a_v (T_s - T_f) + S_{cs}, \tag{2}$$

where x_i and t refer to the space and time coordinates, c_f, c_s are the fluid and solid specific heats, u_i is the average velocity of the fluid (averaged over a channel cross section), α the heat transfer coefficient from the channel walls to the fluid, and a_V the specific surface area (wall surface/reactor volume). Throughout this article, the Einstein convention of summation over repeated indices is assumed. The fluid and solid densities are volume-averaged quantities and given as

$$\rho_f = \Phi_f \rho_f^{(0)}, \qquad \rho_s = \Phi_s \rho_s^{(0)}, \tag{3}$$

where the superscript (0) indicates the corresponding material densities. The equation for the fluid temperature contains source term S_{cf} and S_{cs} which could, for example, represent the input of thermal energy from a chemical reaction. Having source terms in both the fluid and the solid equation leaves open the possibility of studying homogeneous ($S_{cs} = 0$) and heterogeneously catalyzed reactions ($S_{cf} = 0$), where heat is generated in a catalyst attached to the wall. Owing to the anisotropy of the solid matrix, the thermal conductivity is direction-dependent. For this reason a thermal conductivity tensor k_{ij} appears in Eq. 2. The heat transfer coefficient α can

be obtained from well-known correlations for rectangular channels.[20] If entrance flow effects can be neglected, which is the case in a number of practical situations, the value of α is position-independent. Otherwise the enhanced heat transfer in entrance flows might be parametrized as a z-dependence of the heat transfer coefficient. Besides in the thermal conductivity tensor and in the heat transfer coefficient, information about the geometry and the characteristic scale of the microchannel domain is contained in the quantity a_V. The specific surface area plays a key role in determining the speed of heat transfer, but is not generic for the reactor geometry since a variety of geometries can be mapped onto the same a_V. It should also be mentioned that in this work no attempt is made to incorporate specific micro- and nanoscale transport effects, such as slip-flow or temperature jump at the channel walls.[21] These effects may be of relevance when the channel diameter becomes very small (of the order of 1 μm) and require a modification of the heat transfer coefficient with respect to its classical value in macroscopic systems.

The model of Eq. 2 can be regarded as a mean-field model expected to describe the average temperatures of the fluid and the solid phase without incorporating the local fluctuations which are because of temperature gradients within single channels or channel walls. It may be derived from the full transport equations using an averaging approach described by Kaviany.[19]

To clarify whether or not it is justified to omit the axial heat conduction term in the fluid, the following order-of-magnitude inspection may be employed. The conductive term in the energy equation for the fluid is given by $k_f (\partial^2/\partial z^2)T_f$, the convective term by $\rho_f c_f u_z (\partial/\partial z)T_f$, where k_f is the thermal conductivity of the fluid. Assuming an extension of the multichannel stack in z-direction of L_z, the order of magnitude of the conductive and the convective term is $k_f\theta/L_z^2$ and $\rho_f c_f u_z\theta/L_z$, respectively, where θ is a characteristic temperature scale. The ratio of the conductive and the convective term is then given as $1/\mathrm{Pe}_L$ with Pe_L being the Péclet number, which has been computed using the channel length L_z as length scale. Reformulation to quantities with the hydraulic channel diameter d as length scale gives $1/\mathrm{Pe}_L = (d/L_z)1/\mathrm{Pe}_d = (d/L_z)1/\mathrm{Re}_d Pr$. For typical microreactors and corresponding processes, the orders of magnitude of the different terms in this expression are given as $d/L_z \approx 10^{-2}$, $\mathrm{Re}_d \approx 10^1$, $\mathrm{Pr} \approx 1$, yielding a ratio of the conductive and the convective term of 10^{-3}. This conservative estimate is based on gas flow in microchannels of about 100 μm hydraulic diameter and shows that axial heat conduction in the fluid phase may usually be safely neglected, compared with convection. The suppression of axial heat conduction is a manifestation of the well-known result that this effect may be neglected in the limit $\mathrm{Pe}_L \to \infty$. There are a few exceptional cases where this limit is not approached well enough, for example reactors into which a non-preheated fluid is guided, subsequently getting in contact with the hot entrance region of the reactor and being heated up rapidly while undergoing an exothermic reaction.[22,23]

The velocity field u_i may depend on the downstream position inside the reactor, as in the case of a gas-phase reaction, which does not conserve the number of molecules. Then the convection–diffusion-reaction equations for species concentration have to be solved in combination with Eqs. 2 to determine the velocity field in the reactor volume for given inlet conditions. In this work, however, it is assumed that the velocity field is known a priori in the whole reactor volume, and only the equations for the temperature fields are solved. There are specific situations where a priori knowledge about the velocity field in the reactor is available. If the pressure barrier due to the microchannels is large enough, the flow will distribute almost equally over the different channels. In streamwise direction, the velocity will remain approximately constant if the chemical reaction conserves the number of molecules and the temperature variation is small compared to the average absolute temperature in the reactor, an assumption which is fulfilled in many practical cases. It should, however, be noted that the model of Eqs. 2 can be supplemented by a momentum equation which, similar to the energy equation, is obtained from a description based on interpenetrating continua. Such an approach would allow evaluating the spatial dependence of the velocity field, especially in the x–y plane, and would enable the study of changes in the velocity distribution, for example, when the device dimensions are varied in the framework of a parameter study. Owing to the added complexity the implementation and analysis of a correspondingly extended model are left to a forthcoming publication.

In any case, both the heat transfer coefficient and the velocity field are key ingredients of the model presented here and are crucial for the accuracy of the results. The heat source (or sink) is located in the fluid phase, and first the heat needs to be transported from the fluid to the solid phase before it is further conducted through the network of channel walls. The time scale for this initial step is proportional to α^{-1}, while the residence time in a channel is proportional to ${u_z}^{-1}$. Correspondingly, the number of transfer units for heat transfer between the fluid and the solid phase is proportional to α/u_z, thus underlining the impact of these two quantities on the overall accuracy of the results.

A main component of the model governing conductive heat transport is the thermal conductivity tensor k_{ij}, which depends on the geometry of the channel walls. To a good approximation, the multitude of walls shown in Figure 1 can be regarded as a network of thermal resistors (for a detailed analysis of heat conduction in anisotropic media, see chapter 4 of the book by Sahimi[24]). A resistor element from which the network can be build up is shown in Figure 2. To determine the resistances of such an element in x- and y-direction, a series arrangement of two sections of different cross-sections is considered. In x-direction, the resistor comprises one section of length w_f and width h_s and one section of length w_s and width $h_s + h_f$. In y-direction, the corresponding segments have a length of h_f, h_s and a width of w_s and $w_s + w_f$, respectively. In z-direction, the thermal conductivity is simply determined by the area fraction (equaling the volume fraction) of solid material, bearing in mind that the fluid is assumed to have zero conductivity. Based on the resistor elements, the components of the thermal conductivity tensor are derived as

$$k_{xx} \approx (w_f + w_s)\left(\frac{h_f + h_s}{h_s} w_f + w_s\right)^{-1} k_s,$$

$$k_{yy} \approx (h_f + h_s)\left(\frac{w_f + w_s}{w_s} h_f + h_s\right)^{-1} k_s,$$

$$k_{zz} \approx \Phi_s k_s, \quad (4)$$

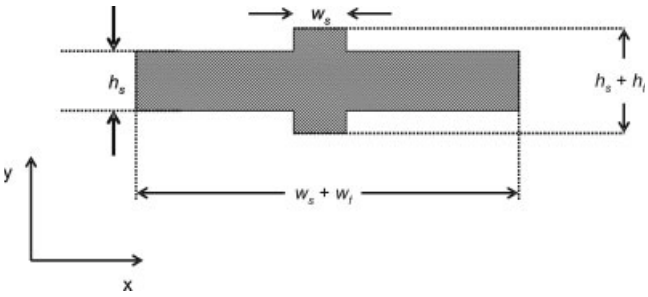

Figure 2. Thermal resistor element from which the walls of the multichannel stack can be built up.

The projection onto the x–y plane is shown.

where k_s represents the thermal conductivity of the solid material. All other components of the thermal conductivity tensor vanish in the chosen reference frame.

In the geometry sketched in Figure 1, the microchannel network forms a structure periodic in the x–y plane, i.e. the same unit cell containing a channel surrounded by solid walls is repeated to form the complete structure. However, the model presented in Eqs. 2 is not limited to such periodic structures and can as well be applied to situations where the channel diameter, aspect ratio, and wall geometry change as a function of x and y. For this purpose, a x and y dependence of the heat transfer coefficient α, the surface-to-volume ratio a_V, and the thermal conductivity tensor k_{ij} may be introduced, reflecting the geometrical changes in the multichannel domain.

In many practical cases only the stationary limit of Eqs. 2 with time derivatives set to zero has to be considered. Owing to the negligible heat conduction in the fluid phase, the transport equations in the two phases are of different nature. Heat transfer in the solid is governed by a second-order PDE, and in order to uniquely determine the temperature field, appropriate thermal boundary conditions have to be defined on a closed surface. In contrast to that, transport of heat in the fluid phase is described by a first-order PDE, and integration along the streamlines of the flow suffices to determine the temperature field. The fluid flow inside the microchannels is in z-direction, that is, the velocity field u_i only has a z-component. Then the PDE for the fluid phase becomes an ordinary differential equation of the form

$$\frac{\partial}{\partial z} T_f = -\lambda T_f + S'_{cf}, \tag{5}$$

with

$$\lambda = \frac{\alpha a_v}{\rho_f c_f u_z}, \qquad S'_{cf} = \frac{\alpha a_v T_s + S_{cf}}{\rho_f c_f u_z}. \tag{6}$$

If λ can be assumed as z-independent, the solution is given by

$$T_f = e^{-\lambda z}\left(C_1 + \int_0^z e^{\lambda z'} S'_{cf}(z')dz'\right), \tag{7}$$

where C_1 is a constant of integration. Usually, the fluid temperature T_{in} at the inlet to the multichannel stack is known. Then $C_1 = T_{in}$, which may still vary as a function of x and y. Equation 7 expresses the fluid temperature as a function of the solid temperature. When inserting this expression into the PDE for the solid phase, a closed equation for the solid temperature is obtained which reads

$$\frac{\partial^2}{\partial x_i^2} k_{ii} T_s = \alpha a_v (T_s - e^{-\lambda z} T_{in}) - e^{-\lambda z} \int_0^z \lambda e^{\lambda z'} (\alpha a_v T_s + S_{cf}) dz' - S_{cs}. \tag{8}$$

The price for eliminating the fluid temperature is the more complicated structure of this equation, which is of integro–differential type. When taking the derivative with respect to z, again a pure differential equation is obtained which reads

$$\left(\lambda + \frac{\partial}{\partial z}\right) \frac{\partial^2}{\partial x_i^2} k_{ii} T_s = \alpha a_v \frac{\partial}{\partial z} T_s - \lambda S_{cf} - \frac{\partial}{\partial z} S_{cs}. \tag{9}$$

Hence, the conjugate heat transfer problem between the solid and the fluid in a multichannel stack reduces to a third-order differential equation for the solid temperature together with Eq. 7 from which the fluid temperature can be obtained. It is conceivable that in a number of situations Eq. 9 is more accessible to numerical approaches or analytical approximations than its counterpart, Eqs. 2.

To uniquely determine the temperature field, boundary conditions have to be defined on the planes $z = 0$, $z = L_z$, $x = \pm L_{x/2}$, $y = \pm L_{y/2}$. In many cases, a realistic choice of boundary conditions could be $\partial/\partial z T_s|_{z=0} = \partial/\partial z T_s|_{z = L_z} = 0$, $T_s|_{x=\pm L_{x/2}} = T_s|_{y=\pm L_{y/2}} = T_0$, with a fixed temperature T_0. The condition of vanishing temperature gradients at $z = L_c$ reflects a scenario where the channels are long enough or the flow velocity is small enough to allow to neglect heat conduction at the channel exits, an assumption that is fulfilled in many practical situations. However, any other set of consistent boundary conditions is admissible. Solving Eq. 9 for the z-dependence of T_s involves three constants of integration (which are actually not constant since they may be functions of x and y because of the third-order derivative in z). Two of these constants are to be adjusted such that the boundary conditions at $z = 0$ and $z = L_z$ are fulfilled. The third constant needs to be chosen such that Eq. 8 is satisfied, which is not equivalent to Eq. 9 but has been used to derive it. For this reason, not every solution of the third-order PDE automatically fulfils the initial integro–differential equation.

Numerical Solution and Validation

Formally, Eq. 9 is easier to solve than the system of equations Eq. 2. The advantage of Eq. 2, however, is the (convection)–diffusion type structure which makes the model accessible to numerical solution by standard CFD tools. Virtually all state-of-the-art CFD tools offer an Euler–Euler model for multiphase flows.[25] Briefly, the idea of such Euler–Euler models is to treat two phases as interpenetrating continua occupying certain volume fractions of the flow domain. The phases can exchange momentum, heat, and matter via source terms appearing in the respective transport equations. The

results to be presented in this section have been obtained with commercial CFD tools based on the Euler–Euler description. In this context, a vanishing velocity was chosen for the solid phase and a constant velocity in z-direction u_0 for the fluid phase. The velocity fields were regarded as fixed, predetermined quantities. The exchange of heat was modeled via the exchange terms appearing in Eq. 2. Throughout this section it is assumed that the reactor contains repetitive channel structures, that is, α, a_v, and k_{ij} are fixed, spatially independent quantities. Usually, the standard Euler–Euler models for two-phase flow do not allow incorporation of an anisotropic thermal conductivity. However, by rescaling the x and y coordinates the anisotropy can be eliminated. For this purpose, the second equation of Eq. 2 is rewritten as

$$\rho_s c_s \frac{\partial}{\partial t} T_s = k_{zz} \left(s_x \frac{\partial^2}{\partial x^2} + s_y \frac{\partial^2}{\partial y^2} + \frac{\partial^2}{\partial z^2} \right) T_s - \alpha\, a_v (T_s - T_f) + S_{cs}, \tag{10}$$

with $s_x = k_{xx}/k_{zz}$, $s_y = k_{yy}/k_{zz}$ and making use of the diagonal structure of the thermal conductivity tensor. By introducing rescaled coordinates $\tilde{x} = x/\sqrt{s_x}$, $\tilde{y} = y/\sqrt{s_y}$, the system of transport equations to solve becomes

$$\rho_f c_f \left(\frac{\partial}{\partial t} + u_0 \frac{\partial}{\partial z} \right) T_f = -\alpha\, a_v (T_f - T_s) + S_{cf}$$

$$\rho_s c_s \frac{\partial}{\partial t} T_s = k_{zz} \left(\frac{\partial^2}{\partial \tilde{x}^2} + \frac{\partial^2}{\partial \tilde{y}^2} + \frac{\partial^2}{\partial z^2} \right) T_s - \alpha\, a_v (T_s - T_f) + S_{cs}, \tag{11}$$

where now the computational domain spans the region defined by

$$-\frac{L_x}{2\sqrt{s_x}} \le \tilde{x} \le \frac{L_x}{2\sqrt{s_x}}, \quad -\frac{L_y}{2\sqrt{s_y}} \le \tilde{y} \le \frac{L_y}{2\sqrt{s_y}}, \quad 0 \le z \le L_z. \tag{12}$$

As a specific model geometry, the multichannel reactor shown in Figure 1 is considered. The reactor comprises 160 microchannels with a depth h_f of 80 μm. The other dimensions characterizing the channel and wall cross section are $h_s = 120$ μm, $w_f = 500$ μm, and $w_s = 80$ μm. The external dimensions of the model are $L_x = 4.64$ mm, $L_y = 4.0$ mm, and $L_z = 9.50$ mm. The archetype for this model is a microreactor for the partial oxidation of ethylene developed at the Institute of Microtechnology Mainz, Germany. The material and operation parameters for the simulations discussed in this section were chosen compliant with the existing reactor and its operation modes. A gas with the properties of nitrogen at 300°C (573.15 K) and 5 bar[26] is assumed to enter the reactor in positive z-direction with a velocity of 1.54 cm/s. The thermal conductivity of the wall material was set to 20 W/(m K), a typical value for stainless steel. The energy input from exothermic chemical reactions occurring in the reactor was modeled by introducing a source term (power/reactor volume) of $S_{cf} = 2.16 \times 10^9$ W/m^3 in a slab extending from the entrance plane up to 1 mm downstream, while $S_{cs} = 0$. That way a very fast reaction with spatially heterogeneous energy input should be mimicked in a simplified way, and its consequences on the temperatures in both the fluid and the solid phase should be studied.

In the mean-field model, reflection symmetry with respect to $x \to -x$ and $y \to -y$ was utilized (Figure 1), and a computational domain with extensions

$$0 \le \tilde{x} \le \frac{L_x}{2\sqrt{s_x}}, \quad 0 \le \tilde{y} \le \frac{L_x}{2\sqrt{s_y}}, \quad 0 \le z \le L_z \tag{13}$$

was set up, thereby accounting for the anisotropy of heat conduction in the solid matrix. The thermal boundary conditions were chosen compliant with the implementation of Euler–Euler models in commercial CFD tools and are summarized as follows

$$\left.\frac{\partial T_i}{\partial \tilde{x}}\right|_{\tilde{x}=0} = 0, \qquad T_i\big|_{\tilde{x}=\frac{L_x}{2\sqrt{s_x}}} = T_0$$

$$\left.\frac{\partial T_i}{\partial \tilde{y}}\right|_{\tilde{y}=0} = 0, \qquad T_i\big|_{\tilde{y}=\frac{L_y}{2\sqrt{s_y}}} = T_0,$$

$$\left.\frac{\partial T_i}{\partial z}\right|_{z=0} = \left.\frac{\partial T_i}{\partial z}\right|_{z=L_z} = 0 \tag{14}$$

where the subscript i refers to either the fluid or the solid phase and $T_0 = 300$°C (573.15 K). The heat transfer coefficient α determines the thermal coupling between the two phases and was computed from the correlation for rectangular channels given by Shah and London.[27]

The numerical solution of the mean-field equations was performed using the commercial finite-volume solver Fluent 6.1 (Fluent). A structured Cartesian computational grid of 19,125 cells was set up with an increased cell density towards the entrance plane in order to account for the steep temperature gradients found in this region, owing to the spatial distribution of the source term. With the fluid velocity given, only Eqs. 11 had to be solved. The QUICK differencing scheme[28] was used for discretization of the convective term.

To benchmark the results of the mean-field model, a full simulation based on an explicit modeling of the geometric structure of the channel walls was performed. For this purpose, a computational domain of the same extent as defined in Eq. 13 was set up, that is, a quarter of the complete multichannel stack with 160 channels was modeled. The same thermal boundary conditions as in Eq. 14 were used. For the fluid phase, the incompressible Navier–Stokes equation was solved in combination with the energy equation

$$\rho_f^{(0)} c_f u_i \frac{\partial}{\partial x_i} T_f = k_f \nabla^2 T_f + S_{cf}, \tag{15}$$

both in their stationary limit.

In the solid phase, only the heat conduction equation

$$\nabla^2 T_s = 0 \tag{16}$$

was solved, demanding continuity of the temperature fields and the heat fluxes at the channel walls. At the inlets to the

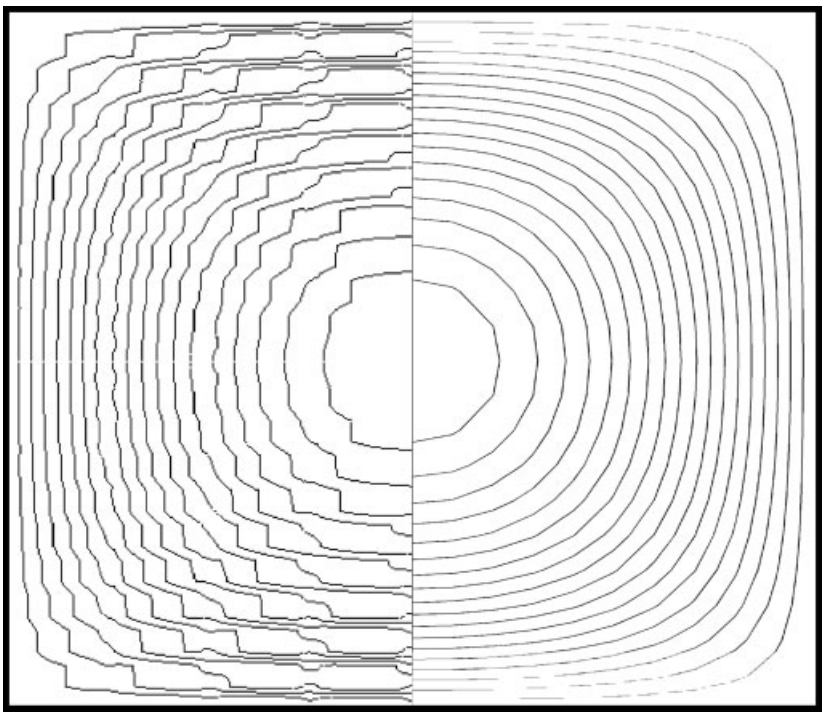

Figure 3. Temperature contour plot in a plane z = const. = 2 mm, as obtained with the full (left) and the mean field model (right).

An inlet velocity of 1.54 cm/s, a temperature of 300°C at the envelope of the stack and a power density of $2.16 \cdot 10^9$ W/m^3 in the heated section of the reactor were assumed.

channels a velocity of 1.54 cm/s was imposed, and a constant-pressure boundary condition was used at the channel outlets.

To resolve the geometric features of the model, a quite large computational grid is required. A grid resolution of 120 $\times$ 160 $\times$ 98 cells was chosen in x, y, and z direction, respectively, amounting to a total of about 1.9 million cells within a structured Cartesian grid. In a similar way as in the mean-field model, biased subdivisions in z-direction were defined to better resolve the temperature gradients close to the entrance plane of the reactor. The full simulation was performed using the commercial finite-volume solver CFX5.7 (ANSYS CFX). For discretization of the convection term in both the momentum and the heat transport equation, a flux-corrected transport scheme based on the work of Barth and Jespersen[29] for unstructured grids was used. The solution of the system of nonlinear algebraic equations obtained after discretization was performed with a fully coupled solver, treating the different equations for conservation of mass, momentum, and energy on an equal basis. For this reason, no separate pressure–velocity coupling scheme had to be specified. The systems of linear algebraic equations obtained within the nonlinear iteration scheme were solved with the help of the algebraic multigrid method.[30]

Typical temperature distributions obtained with both models are shown in Figure 3. The figure displays temperature contour lines over a cross section of the reactor in a plane with $z = 2$ mm, on the left side those of the full, on the right side those of the mean-field model. Eighteen contour lines are equidistantly spaced between a minimum temperature of 573.15 K and a maximum temperature of 580.92 K. At this position in the reactor, the solid and fluid phase contour lines obtained with the mean-field model are indistinguishable. As expected, the contour lines of the mean-field model are smoother than those of the full model. The reason for the kinks in the contour lines of the full model are the very different thermal resistances of the fluid and the solid phase, leading to very small temperature gradients in the solid walls as compared with the fluid. The overall agreement of the two different descriptions is good and indicates that the mean-field model provides a reasonable approximation to the complete picture.

A comparison of the two models in form of a x–y plot is shown in Figure 4. On the top of the figure, the data for the solid temperature are displayed, on the bottom those for the fluid temperature. The curves show the temperatures along a straight line located at $x = 0$, $y = 0$, that is, the temperature profiles in flow direction. As there is no fluid channel at this location, the data for the full model have been obtained by averaging the temperature in the channel closest to $(x,y) = (0,0)$. The results show that in the entrance region to the multichannel stack, the fluid temperature deviates from the solid temperature in both the full and the mean-field model, thus justifying a description going beyond a thermal-equilibrium scenario. The difference between the two temperature levels is smaller in the full model, probably because of the enhanced heat transfer in hydrodynamically and thermally developing flows, which has not been implemented in the

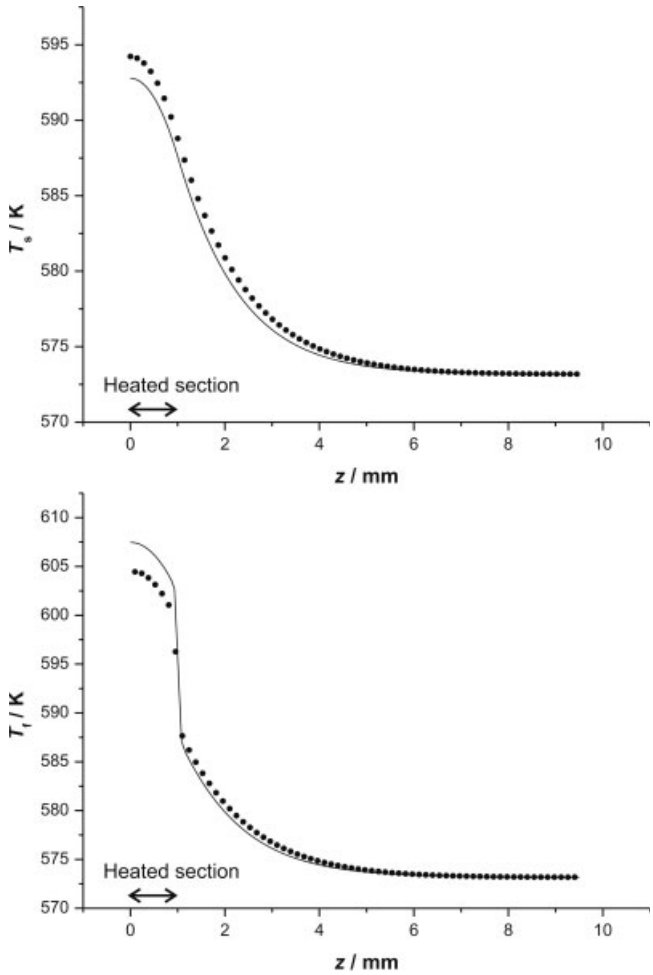

Figure 4. Solid (top) and fluid (bottom) temperatures along the flow direction as obtained from the full (dots) and the mean field model (lines).

The data have been evaluated in the center of the reactor at $x = y = 0$. The conditions were the same as those described in Figure 3.

mean-field model. Inclusion of a locally increasing heat transfer coefficient in the entrance region of the reactor may also improve the agreement between the two models for $z <$ 1 mm. Owing to the more efficient heat transfer in the solid (compared with that in the fluid, which is characterized by an additional resistance because of the fluid-solid heat transfer), the temperatures in the solid are lower than those in the fluid. Overall, the agreement between the two model predictions is satisfactory, with local differences in temperature of about 3 K at maximum and a total temperature range of about 35 K.

A second comparison is shown in Figure 5. The top of the figure shows the temperatures in the solid plotted along the z-direction for $x = 1.16$ mm and $y = 0$. On the bottom, a temperature plot along the y-direction is displayed, with $x =$ 0.29 mm and $z = 2$ mm. The direction vector of this plot lies in the symmetry plane of first column of channels counted from the center of the reactor. The top of the figure shows a good agreement, thus indicating that also for off-center plots along the z-direction the mean-field model approximates the temperature field quite well. On the bottom of Figure 5, the mean-field curve follows the full-model data only very roughly. At such a distance from the entrance plane, the fluid and the solid temperatures have equilibrated such that only a single line is necessary to represent the results of the mean-field model. The zig-zag-shape of the temperature field obtained from the full model is due to the line cutting through both fluid and solid volumes, where the almost horizontal segments of the temperature curve represent the solid. In spite of the at first sight unsatisfactory comparison of this profile with the mean-field data, it should be noted that the absolute deviations between the two data sets are rather small, amounting to less than 1.5 K.

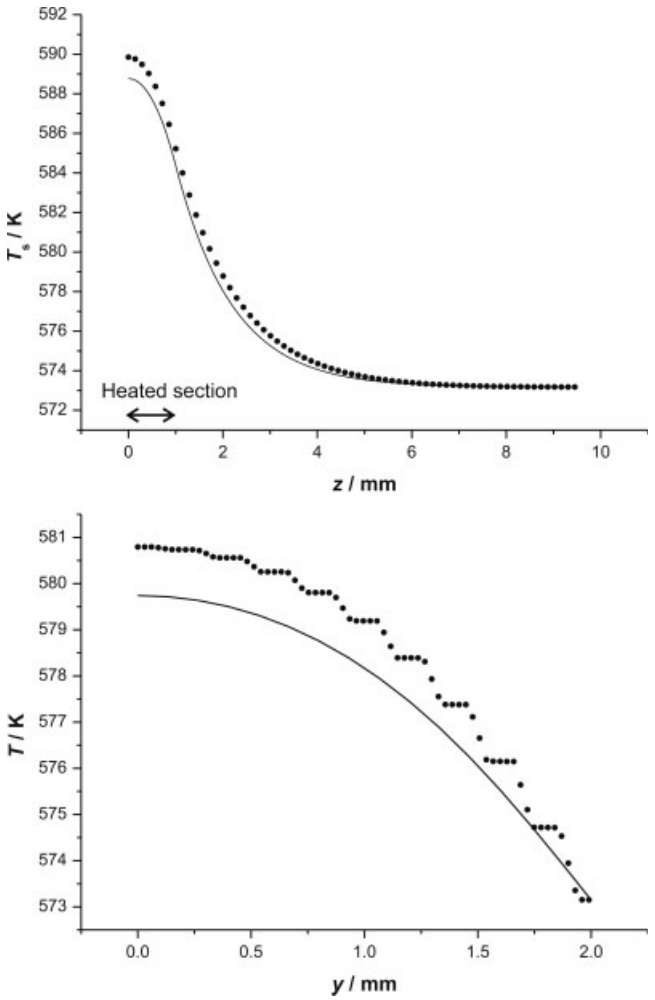

Figure 5. The top of the figure shows the solid temperature as a function of z at x = 1.16 mm and y = 0. On the bottom, temperature is plotted along the y-direction at x = 0.29 mm and z = 2 mm.

Dots indicate the full-model, lines the mean-field data. The conditions were the same as those described in Figure 3. The positions at which the plots in z- and in y-direction have been created are indicated in Figure 1.

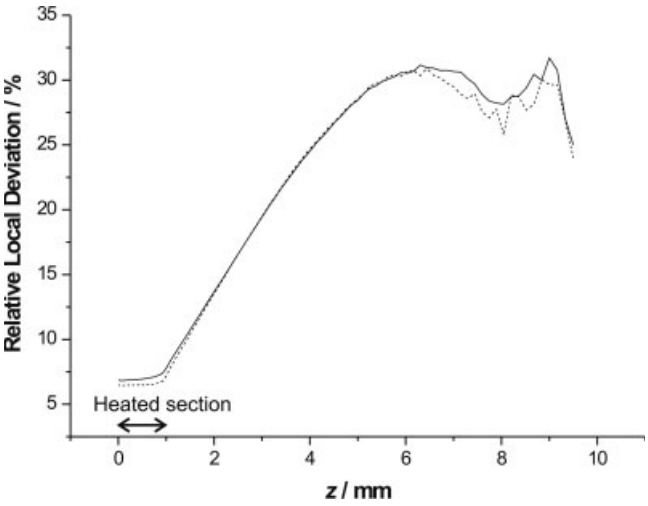

Figure 6. Relative deviation between the full and the mean-field model as a function of z for (x,y) = (0,0) (solid line) and (x,y) = (1.16 mm, 0) (dashed line).

The conditions were the same as those described in Figure 3.

The relative local deviation between the two models being defined as

$$\Delta T_{\mathrm{loc}} = \frac{\left|T^{(\mathrm{full})} - T^{(\mathrm{mf})}\right|}{T^{(\mathrm{full})} - T_0} \tag{17}$$

is displayed in Figure 6 as a function of the z-coordinate. Here, the temperatures in the solid are compared and the same points in the x–y plane as in Figures 4 and 5 have been chosen. The two different curves look very similar and virtually lie on top of each other. In the entrance region, the local temperature deviation is about 7% and grows to about 30% in the region close to the outlet plane. Note however, that in this region $T^{(\mathrm{full})} - T_0$ has already dropped below 0.5 K.

To check the grid independence of the numerical results, two separate grids with a larger and smaller number of cells than the reference case were set up. In the case of the mean-field model, these grids comprise 5700 and 61,468 cells, respectively. For the full model, the corresponding numbers of computational cells are 600,600 and 4,804,800. Figure 7 displays the fluid and solid temperature profiles along a line in z-direction cutting through the center of the multichannel stack for different grid resolutions. The figure shows very little deviation between the results obtained with the reference grids (dotted curve) and the results of the coarser (dashed curve) and finer (solid curve) grids. In the case of the mean-field model, the different curves are not even distinguishable. This shows that the grid resolution chosen is large enough to compute the temperature field within the reactor with sufficient accuracy.

One may argue that the results presented so far are quite specific, since they relate to the reactor geometry shown in Figure 1. To explore the limits of validity of the developed model for reactors with a smaller number of channels, a total of seven different multichannel stacks with 20, 16, 12, 8, 6, 4, and 2 platelets with microchannels were considered. The model with 20 layers corresponds to the original geometry shown in Figure 1, in the other cases the number of layers in y-direction is reduced, with the height of the multichannel stack L_y being reduced accordingly. Since the mean-field approach described in this article is based on an averaging procedure over the microscopic geometrical features (the channels and the channel walls), it is expected that the quality of the approximation deteriorates as the number of layers is reduced. As a measure for the discrepancy between the full and the mean-field model results, an absolute deviation is introduced as

$$\Delta T_{\mathrm{abs}} = \frac{1}{L_z}\int_0^{L_z}\left|T^{(\mathrm{full})} - T^{(\mathrm{mf})}\right| dz. \tag{18}$$

The integral in z-direction is to be evaluated at $x = y = 0$, that is, in the center of the reactor which belongs to the solid

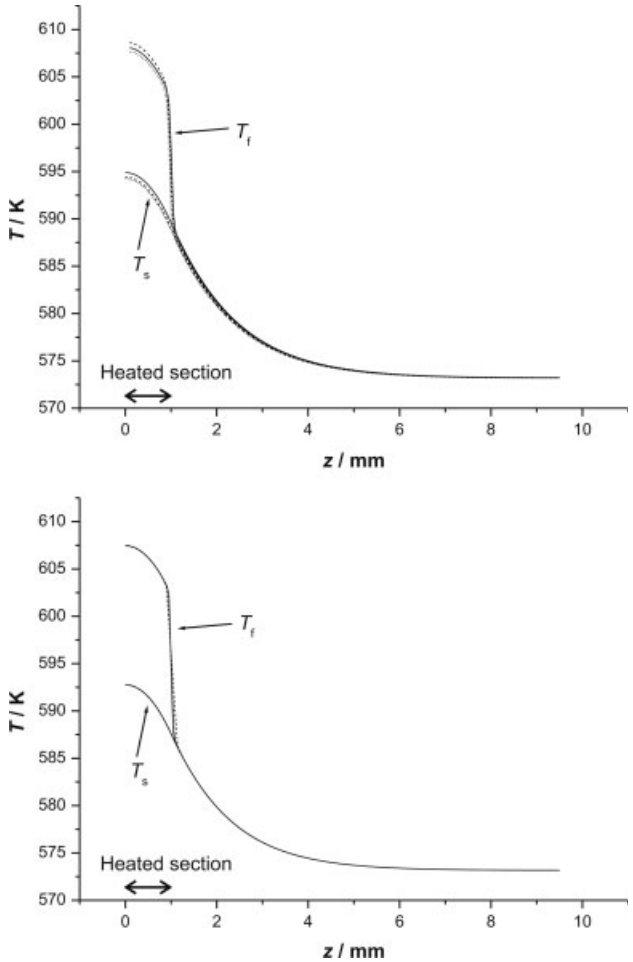

Figure 7. Solid and fluid temperatures in the center of the reactor as computed with the reference (dotted curves), coarser (dashed curves), and finer grids (solid curves).

The top of the figure shows the results of the full model, the bottom those of the mean-field model. The conditions were the same as those described in Figure 3.

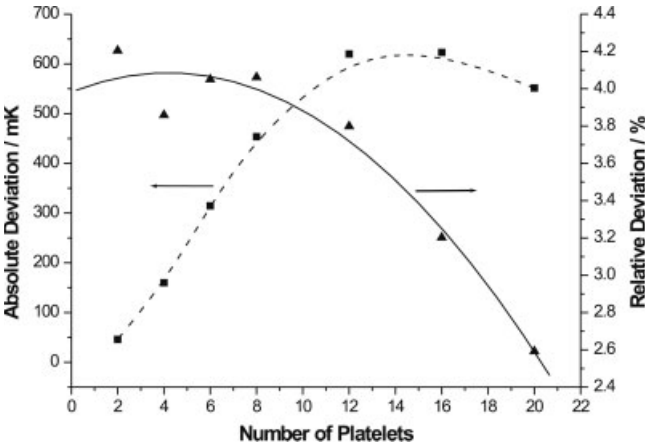

Figure 8. Absolute and relative temperature deviation between the full and the mean-field model evaluated by integration in *z*-direction at (*x*,*y*) = (0,0).

The squares and dashed line show the absolute, the triangles and the full line the relative deviation. The conditions were the same as those described in Figure 3.

domain. The corresponding relative deviation is obtained via dividing Eq. 18 by the maximum temperature difference $|T_{max} - T_0|$, where T_{max} is the maximum temperature obtained with the full model for $x = y = 0$.

In Figure 8 the absolute and relative temperature deviations are plotted as a function of the number of platelets. The data points are fitted by a second-order polynomial (solid line) and a B-spline (dashed line). The absolute temperature deviation decreases with a decreasing number of platelets. However, with fewer and fewer platelets the reactor becomes increasingly flatter, resulting in a simultaneous decrease of the absolute temperature difference as defined above. Thus, even with a decreasing absolute temperature deviation, the relative deviation increases when the number of platelets is reduced, leveling off at a value of about 4%. From Figure 8 it can be estimated how the developed mean-field model performs in cases where the number of channels is so small that the underlying averaging approach hardly appears to be justified. The smallest reactor (two platelets) has only 16 channels, still the relative temperature deviation is limited to about 4%.

The close similarity of the computational results of the two models stands in sharp contrast to the respective computational efforts. Referring to the grid dependence shown in Figure 7, it seems appropriate to compare the smallest grid of the mean-field model with the largest grid of the full model, since the mean-field model results remain virtually unchanged under grid refinement. Under this assumption, the solution of the full model takes about 7 h on three 3-GHz-Intel Xeon processors. In contrast, only a few seconds were required to obtain a solution for the mean-field model on one 3-GHz-Intel Pentium processor. Thus, the computation times differ by a factor of a few thousand, a point to pay attention to when a fast evaluation of reactor designs is required in the context of parameter studies or optimization runs. Even when the velocity field is not computed but prescribed, and only the temperature field is solved for within the full model, the difference in computational burden is still dramatic. Simply from the number of grid cells ($\approx$6000 for the mean-field, $\approx$5 million for the full model) a speed up factor of several hundred can be derived.

It is also instructive to compare the computational costs of the full and the mean-field model as a function of the number of channels N. Based on the constraint that the number of grid cells needed to resolve a single channel is a fixed quantity, the total number of cells required for the full model scales as N, whereas in the mean-field model (where channel geometries no longer need to be resolved explicitly), the total number of cells is independent of N. For very large N, the computational savings of the mean-field model may even be bigger than that, because when the outer dimensions of the multichannel stack are kept fixed and the number of channels increases, the aspect ratio of the grid cells in the full model increases simultaneously. It may therefore be necessary to define a single-channel grid with a larger number of cells in order to keep the aspect ratio within reasonable limits.

Summary and Conclusions

A 3-D mean-field model has been developed allowing for a fast computation of the temperature field in multichannel microreactors. The model treats the reaction fluid and the wall material as interpenetrating continua which can exchange heat via a prescribed heat transfer coefficient characteristic for the channel cross section under consideration. Heat conduction within the channel walls is represented by a thermal conductivity tensor, whose components contain information on the specific wall geometry. It was shown that the fluid temperature can be eliminated from the set of partial differential equations, leading to a closed equation for the solid temperature.

The numerical solution of the mean-field model was performed for a test case inspired by a specific practical application, namely the partial oxidation of ethylene. Parallel to that, a more detailed model—the so-called full model—was set up. The full model accounts for the geometric structure of the microreactor explicitly and fully resolves the details of channel geometry. Consequently, the full model contains a far larger number of degrees of freedom. A comparison of the temperature profiles between the mean-field and the full model shows a satisfactory agreement. Both models indicate that in the entrance region of the reactor the fluid and the solid temperatures are not equilibrated, thus underlining the necessity of a two-temperature model. The reason for this local deviation from thermal equilibrium is the fast chemical reaction, which inputs heat into the fluid being subsequently transferred to the channel walls.

The times needed to numerically solve the equations of the two models are strikingly different. A speed-up factor of several hundred to a few thousand can be achieved with the mean-field model, depending on whether or not the momentum and mass conservation equations are solved. This makes the mean-field description an especially promising method for the fast evaluation of reactor designs. When developing a microreaction system, it is often unclear how exactly the properties of the channel walls (geometry and thermal conductivity) influence the reaction performance. Usually the goal is to achieve a temperature distribution as uniform as possible, in order to suppress unwanted side reactions and to

increase the selectivity of the process. Because of its reduced computational cost, the mean field model presented in this article should allow to compare the thermal performance of different reactors, perform parameter studies, and optimization runs, and thereby identify favorable designs.

Notation

a_V = specific surface area, m^2/m^3
c = specific heat, J/(kg K)
C_1 = constant of integration, K
d = hydraulic diameter of microchannel, m
h = channel depth, m
k_f = fluid thermal conductivity, W/(m K)
k_{ij} = thermal conductivity tensor W/(m K)
k_s = solid thermal conductivity W/(m K)
L = extension of model domain, m
N = number of microchannels
Pe = Péclet number
Pr = Prandtl number
Re = Reynolds number
S_{cf} = heat source in fluid, W/m^3
S_{cs} = heat source in solid, W/m^3
s_x = ratio of thermal conductivities
s_y = ratio of thermal conductivities
t = time, s
T = temperature, K
T_0 = temperature at domain boundary, K
ΔT_{abs} = absolute temperature difference, K
ΔT_{loc} = relative local temperature deviation
u_i = fluid velocity, m/s
w = channel width, m
(x, y, z) = (x_1, x_2, x_3)
x_i = spatial coordinate vector, m

Greek letters

α = heat transfer coefficient, $W/(m^2 K)$
Φ = volume fraction
λ = parameter determining temperature derivative, m^{-1}
θ = characteristic temperature scale
ρ = density, kg/m^3

Subscripts

d = based on channel diameter
f = fluid
in = value at inlet plane
L = based on channel length
max = maximum value
s = solid

Superscripts

(0) = referring to material property
$'$ = indicating modified source term or integration variable
(full) = referring to full model
(mf) = referring to mean-field model

Literature Cited

1. Hessel V, Hardt S, Löwe, H. Chemical Micro Process Engineering: Fundamentals, Modelling and Reactions. Weinheim: Wiley-VCH, 2004.
2. Hessel V, Löwe H, Müller A, Kolb G. Chemical Micro Process Engineering: Processing and Plants. Weinheim: Wiley-VCH, 2005.
3. Kaniadakis G, Beskok A, Aluru N. Microflows and Nanoflows. New York: Springer, 2005.
4. Zohar Y. Heat Convection in Micro Ducts. Dordrecht: Kluwer Academic, 2003.
5. Rebrov EV, de Croon MHJM, Schouten JC. Design of a microstructured reactor with integrated heat exchanger for optimum performance of highly exothermic reactions. *Catal Today*. 2001;69:183–192.
6. Kestenbaum H, Lange de Oliveira A, Schmidt W, Schüth F, Ehrfeld W, Gebauer K, Löwe H, Richter T. Silver-catalyzed oxidation of ethylene to ethylene oxide in a microreaction system. *Ind Eng Chem Res*. 2000;41:710–719.
7. Kursawe A, Pilz R, Dürr H, Hönicke D. Development and design of a modular microchannel reactor for laboratory use. In: Proceedings of the 4th International Conference on Microreaction Technology, Atlanta, GA, 2000:227–235.
8. Fichtner M, Mayer J, Wolf D, Schubert K. Microstructured rhodium catalysts for the partial oxidation of methane to syngas under pressure. *Ind Eng Chem Res*. 2001;41:710–719.
9. Stief T, Langer OU, Schubert K. Numerical investigations of optimal heat conductivity in micro heat exchangers. *Chem Eng Technol*. 1999;21:297–302.
10. Maranzana G, Perry I, Maillet D. Mini- and micro-channels: influence of axial conduction in the walls. *Int J Heat Mass Transfer*. 2004;47:3993–4004.
11. Wei X, Joshi Y. Stacked microchannel heat sinks for liquid cooling of microelectronic components. *ASME J Heat Transfer*. 2004;126: 60–66.
12. Koo JM, Im S, Jiang L, Goodson KE. Integrated microchannel cooling for three-dimensional electronic circuit architectures. *ASME J Heat Transfer*. 2005;127:49–58.
13. Kim SJ, Kim D. Forced convection in microstructures for electronic equipment cooling. *ASME J Heat Transfer*. 1999;121:639–645.
14. Kim SJ, Kim D, Lee DY. On the local thermal equilibrium in microchannel heat sinks. *Int J Heat Mass Transfer*. 2000;43:1735–1748.
15. Bracken JE, Sun DK, Cendes Z. Characterization of electromagnetic devices via reduced-order models. *Comput Methods Appl Mech Eng*. 1999;169:311–330.
16. Cangellaris AC, Zhao L. Model order reduction techniques for electromagnetic macromodelling based on finite methods. *Int J Numer Model*. 2000;13:181–197.
17. Bai Z. Krylov subspace techniques for reduced-order modeling of large-scale dynamical systems. *Appl Numer Math*. 2002;43:9–44.
18. Rowley CW. Model reduction for fluids, using balanced proper orthogonal decomposition. *Int J Bifurcat Chaos*. 2005;15:997–1013.
19. Kaviany M. Principles of Heat Transfer in Porous Media. New York: Springer, 1995.
20. Hartnett JP, Kostic M. Heat transfer to newtonian and non-newtonian fluids in rectangular ducts. *Adv Heat Transfer*. 1989;19:247–356.
21. Gad-el-Hak M. The fluid mechanics of microdevices. *J Fluid Eng T ASME*. 1999;121:5–33.
22. Stutz MJ, Poulikakos D. Effects of microreactor wall heat conduction on the reforming process of methane. *Chem Eng Sci*. 2005;60: 6983–6997.
23. Ryi SK, Park JS, Choi SH, Cho SH, Kim SH. Novel micro fuel processor for PEMFCs with heat generation by catalytic combustion. *Chem Eng J*. 2005;113:47–53.
24. Sahimi M. Heterogeneous Materials. I. Linear Transport and Optical Properties. New York: Springer, 2003.
25. Kolev NI. Multiphase Flow Dynamics. Berlin: Springer, 2002.
26. Verein Deutscher Ingenieure, editor, VDI-Wärmeatlas Berlin: Springer, 2002.
27. Shah RK, London AL. Laminar Flow Forced Convection in Ducts. New York: Academic Press, 1978.
28. Leonard BP. A stable and accurate convection modelling procedure based on quadratic upstream interpolation. *Comput Methods Appl Mech Eng*. 1979;19:59–98.
29. Barth TJ, Jespersen DC. The design and application of upwind schemes on unstructured meshes. AIAA, Paper 89–0366, 1989.
30. Hutchinson BR, Raithby GD. A multigrid method based on the additive correction strategy. *Numer Heat Transfer*. 1986;9:511–537.

Manuscript received Nov. 16, 2006, and revision received Jan. 16, 2007.